communications engineering

ARTICLE

https://doi.org/10.1038/s44172-022-00042-3 OPEN

A digital twin of electrical tomography for quantitative multiphase flow imaging

Shengnan Wang[1,2], Delin Hu[1], Maomao Zhang[3], Jiawang Qiu Lin[1], Wei Chen[4], Francesco Giorgio-Serchi[5], Lihui Peng[4], Yi Li[3] & Yunjie Yang[1✉]

Multiphase flow is ubiquitous in nature, industry and research, and accurate flow imaging is critical to understanding this complex phenomenon. Electrical tomography (ET) is a promising technique for multiphase flow visualization and characterization which provides a non-invasive and non-radiative way to unravel the internal physical properties at high temporal resolution. However, existing ET-based multiphase flow imaging methods are inadequate for quantitative imaging of multiphase flows due to inversion errors and limited ground truth data of fluid phases distribution. Here we report a digital twin (DT) framework of ET to address the challenges of real-time quantitative multiphase flow imaging. The proposed DT framework, building upon a synergistic integration of 3D field coupling simulation, model-based deep learning, and edge computing, allows ET to dynamically learn the flow features in the virtual space and implement the model in the physical system, thus providing excellent resolution and accuracy. The proposed DT framework is demonstrated using electrical capacitance tomography (ECT) of a gas-liquid two-phase flow. It can be readily extended to a broader range of tomography modalities, scenarios, and scales in biomedical, energy, and aerospace applications.

[1] SMART Group, Institute for Digital Communications, School of Engineering, The University of Edinburgh, Edinburgh, UK. [2] College of Electrical, Energy and Power Engineering, Yangzhou University, Yangzhou, China. [3] Tsinghua Shenzhen International Graduate School, Shenzhen, China. [4] Department of Automation, Tsinghua University, Beijing, China. [5] Institute for Integrated Micro and Nano Systems, School of Engineering, The University of Edinburgh, Edinburgh, UK. ✉email: y.yang@ed.ac.uk

Multiphase flow, as a transient and dynamic system subject to highly nonlinear and hierarchical multi-scale features, is prevalent in the natural environment, industrial processes and scientific research[1–3]. Representative phenomena include blood flow in blood vessels[4], gas-liquid flow in post-combustion carbon capture processes[5], oil-gas flow in the energy industry[6], and micro-fluidic systems in biomedical research[7]. A critical challenge in this field is the quantitative visualization and characterization of the multiphase flow, which is vital to the fundamental study of the underlying fluid mechanics, the prediction and control of the flow response, process modeling, and the safe operation of industrial facilities[8,9]. Although some imaging techniques, e.g., X-ray tomography[10–12] and Magnetic Resonance Imaging (MRI)[13], can be used to provide quantitative flow images, their viability is severely constrained by their limited versatility, scalability, high cost, and non-negligible radiological hazard. Electrical Tomography (ET), e.g., Electrical Capacitance Tomography (ECT) and Electrical Impedance Tomography (EIT), is considered a promising alternative technology for multiphase flow visualization and characterization[14,15]. It can provide an agile, noninvasive and nonradioactive way to unravel the time-varying distribution of the internal physical properties at high temporal resolution thus facilitating the study of dynamic flow behavior at different scales and under extreme conditions[14,16].

Despite advances in sensors, system design, and inverse problem theory, existing ET techniques are still inadequate for quantitative imaging of multiphase flows[17,18]. The underlying reason is the ill-posed and ill-conditioned nature of the ET inverse problem[19], which leads to inevitable inversion errors. Another issue lies in the limited availability of ground truth data of fluid phases distribution for quantitative image evaluation and validation[20]. This is due to the highly complex nature of multiphase flows, which systematically prevents the time-history recording of accurate flow profiles.

Emerging deep learning and data-driven methods have the potential to resolve the nonlinear ET inverse problem[21,22]. Several learning-based imaging models, e.g., end-to-end learning[23,24], model-based deep learning[25,26], and unsupervised learning[27,28], have been studied for high-resolution ET image reconstruction. The dataset plays a central role in these learning-based imaging approaches and determines the network's accuracy and generalization ability. Since the ground truth of multiphase flow profiles cannot be readily obtained in practice, the datasets of existing learning-based approaches are mainly constructed from static phantom data. Such static datasets are far from actual flow distributions and contain little information on dynamic flow behaviors, making learning-based models unfit to be transferred into realistic multiphase flow imaging scenarios.

We here propose a Digital Twin (DT) framework of ET to achieve quantitative imaging of multiphase flows by encapsulating dynamic 3D field-coupling simulation, model-based deep learning, and edge computing. The DT framework is summarized in Fig. 1. The physical entity includes the testing section of a multiphase flow facility (Fig. 1a), the ET system (Fig. 1b), and the edge computer (Fig. 1c). A three-dimensional Fluid-Electrostatic field Coupling Model (3D-FECM) is developed as the digital representation of the physical multiphase flow imaging system. With 3D-FECM, the dynamic behavior of the real multiphase flows can be modeled, and instantaneous virtual ET measurements can be obtained simultaneously. By conducting dynamic coupling simulations, a virtual dataset consisting of tomographic data and corresponding flow profiles is generated (Fig. 1f). The framework also comprises a lightweight deep neural network (Fig. 1g), i.e., Deep Back Projection (DBP) (see Methods for details), trained based on the dataset and then implemented in the edge computer for quantitative multiphase flow imaging in the physical platform.

The DT framework provides an efficient way for ET to learn the dynamic flow features in the virtual space and enable quantitative multiphase flow imaging in the physical space. The DT framework is demonstrated on ECT and gas-liquid flow in this work but can be readily extended to other electrical tomography modalities, e.g., EIT or magnetic induction tomography, different multiphase flows, e.g., liquid-solid flow, and different scales. By adapting the coupling simulation model to specific cases, the DT framework also can be applied to other multiphase flow imaging techniques. This study provides a paradigm for multiphase flow measurement, extends the limit of ET, and creates an effective avenue for developing artificial intelligence-based quantitative ET techniques.

Results

We first created a three-dimensional Fluid-Electrostatic field Coupling Model (3D-FECM) (see Methods for details of 3D-FECM and Fig. 2b) as the digital representation of the testing section of a pilot-scale multiphase flow facility (see Methods for multiphase flow facility details). In the multiphase flow facility, single-phase flows of gas (air) and liquid (white oil) are separately supplied and controlled to generate gas-liquid flows with different volumetric concentrations (see Fig. 2a). Similarly, in the virtual space, dynamic flows of gas and liquid are separately regulated to simulate various gas-liquid flows. Figure 2c shows examples of typical sequential gas-liquid flows with 0.2 s intervals generated by the 3D-FECM. The pipe is initially filled with liquid. Gas-liquid flows are gradually formed in the horizontal pipe with the gas and liquid injection and then flow through the outlet. Additional representative gas-liquid flows generated from virtual space are presented in Supplementary Movies S1 and S2.

By coupling the fluid and electrostatic fields, the specific electric potential distribution within the virtual ECT sensor is formed, and 66 independent interelectrode capacitances can be obtained during the dynamic simulation process following the ECT measurement principle[29] (see Fig. 2d and Supplementary Fig. S2). To imitate the Signal-Noise Ratio (SNR) of the real-world ECT system, which is around 60 dB[30], three levels of additive noise (SNR 60, 50, and 40 dB) are added to the virtual capacitances when reconstructing the cross-section liquid phase distributions in the sensor region. Referring to the actual working conditions of the multiphase flow testing facility, we conduct large-scale virtual experiments and synthesize a simulation dataset consisting of 12,362 samples of gas-liquid flow distributions and corresponding ECT measurements; see Methods for details of virtual multiphase flow data generation. Several examples of gas-liquid flow distributions and related images reconstructed using the conventional algorithm are shown in Supplementary Figs. S3–4.

We develop a lightweight deep neural network (i.e., Deep Back Projection, DBP) and train the network using the simulation dataset (see Methods for details of DBP). We implement a series of virtual tests (using 50 dB noisy data) to verify the performance of the trained DBP for quantitative gas-liquid flow imaging. We calculate the 2D liquid phase distributions from the 3D liquid phase distributions of the ECT sensing region by averaging voxel-to-voxel along the axial direction of the sensor, and use them as the ground truth (see Fig. 3a). The Structural Similarity Index Measure (SSIM)[31] and the Root Mean Square Error (RMSE)[32] are adopted as the metrics to evaluate the reconstructed flow images quantitatively. Figure 3a presents two representative sets of sequential gas-liquid flows generated by 3D-FECM and

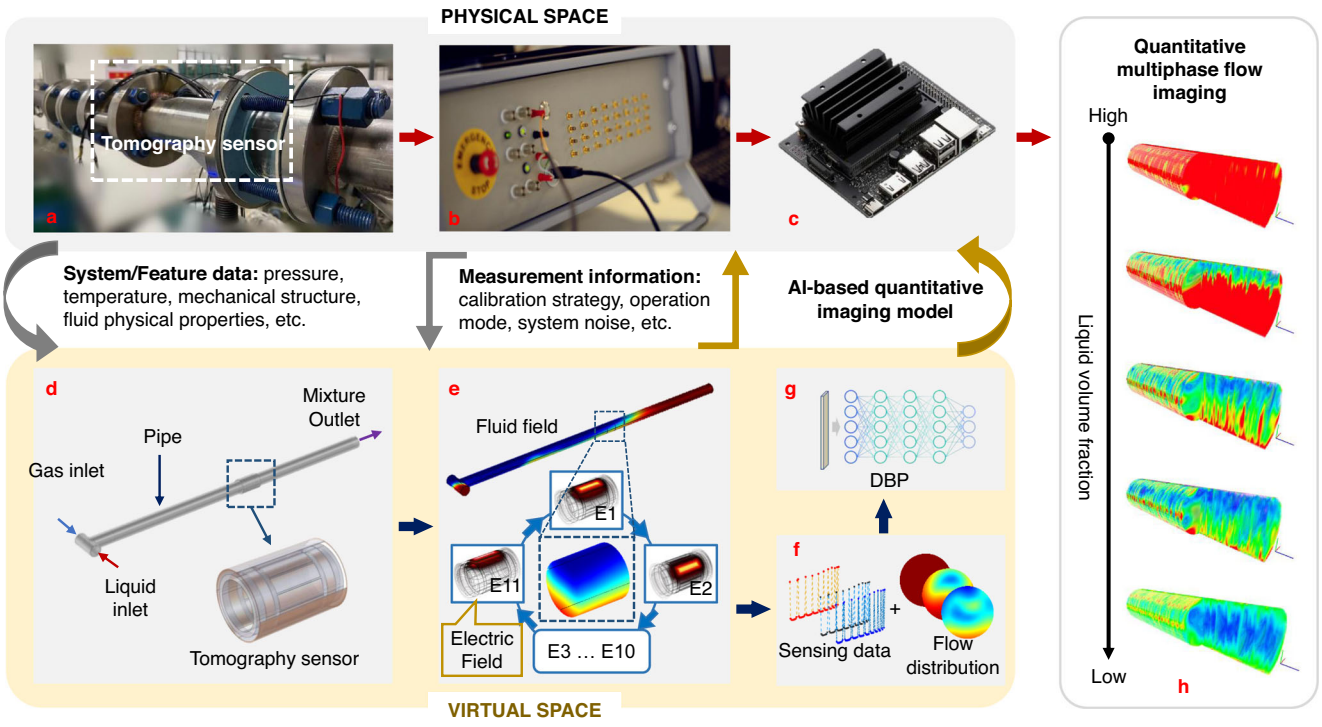

Fig. 1 The digital twin framework of electrical tomography for quantitative multiphase flow imaging. a The testing section of the multiphase flow facility. The system/feature data are captured via the sensors installed in the testing section. **b** The electrical tomography system. **c** The edge computer (i.e., NVIDIA Jetson Nano) implements the AI-based quantitative imaging model. **d** The 3D geometrical model of the testing section and the 12-electrode tomography sensor. **e** Schematic of the 3D fluid-electric field-coupling simulation based on the model in **d**. **f** Illustration of the generated virtual tomographic sensing data and corresponding dynamic flow distributions within the sensing region. **g** The model-based deep neural network, Deep Back Projection (DBP), for quantitative flow imaging. DBP is trained based on the dataset in **f** and implemented in **c**. **h** The edge computer's output generates quantitative flow images and key parameters estimation based on the output of **b**.

corresponding image reconstruction results using DBP when the pipe is initially filled with liquid and gas, respectively. The reconstructed cross-section images from both sets of sequential flows are close to the ground truth, with the SSIM higher than 0.997 and show RMSE lower than 0.014. We also implement virtual gas-liquid transient flow measurement with high temporal resolution (200 frames per second, 0.005 s intervals) to further examine the performance of DBP. Figure 3b shows the image reconstruction results for the set of virtual sequential gas-liquid flows in Fig. 3a (ii), corresponding dynamic imaging results are presented in Supplementary Movies S3.

Additionally, we also uniformly deploy eight virtual ECT sensors on the periphery of the pipeline to image the gas-liquid flows along the whole horizontal pipe section (see Supplementary Fig. S6). The goal is to increase the diversity of flow patterns in the virtual dataset. The image reconstruction results in Fig. 3 and Supplementary Fig. S9 show superior quality with the SSIM higher than 0.989 and RMSE lower than 0.024, indicating that the trained DBP can achieve accurate imaging of a wide variety of complex dynamic gas-liquid flows in the virtual space, which is not possible with the conventional ECT approach (see Supplementary Figs. S7–9 for comparison).

We conduct gas-liquid dynamic flow imaging experiments on the pilot-scale multiphase flow facility as a case study to evaluate the performance of our DT framework (see Methods and Supplementary Table S1 for detailed experimental setups/test matrix). Supplementary Movies S4 presents gas-liquid flows captured by cameras under three experimental conditions, respectively. Some representative flows for the three experimental conditions are shown in Fig. 4a. The pipe is initially filled with liquid. With the gas and liquid injection, stratified gas-liquid flow is gradually presented in the horizontal section and flows through the ECT sensor. When the gas volume flow rate rises from 20.0 to 100.0 $m^3 h^{-1}$ and the liquid volume flow rate drops from 5.0 to 2.5 $m^3 h^{-1}$, the liquid volumetric concentration of the gas-liquid flow in the testing section of the pipe decreases notably. Figure 4b shows the continuous imaging results of the DT framework for each experimental condition. All the tomographic images present stratified flow, and the trend of fluid concentration for different conditions is in good agreement with that from the experimental flow observations. The experiment consists of three stable and two intermediate stages (see Fig. 4b(iv)). According to the tomographic data, the liquid volumetric concentration of the gas-liquid flow at each stage is 0.999 ± 0.003, 0.645 ± 0.097, and 0.221 ± 0.113 (mean ± standard deviation), respectively. The gas-liquid flows at intermediate stages contain more abundant dynamic features than the stable stages that are primarily stratified flows. Two sets of time-stacked tomographic images at intermediate stages are selected and presented in Fig. 4b (v) and (vi), respectively. The flow transitions show similarity compared with simulations, with the Liquid Volumetric Concentration fluctuating within 0.988 to 0.730, and 0.735 to 0.306, respectively. We conduct gas-liquid dynamic flow imaging experiments in virtual space, in line with the physical experimental setup, as validation test case to further verify the reliability of 3D-FECM. Gas Volume Fraction (GVF) is one of the critical parameters describing a gas-liquid flow system, and we calculate the mean value of GVF for each working condition by averaging the continuous measurements in the quasi-static stage. Supplementary Figure S11 compares the GVF results between the simulation and experiment. We can see that the simulation results agree with the experiment across each working condition, and capture the

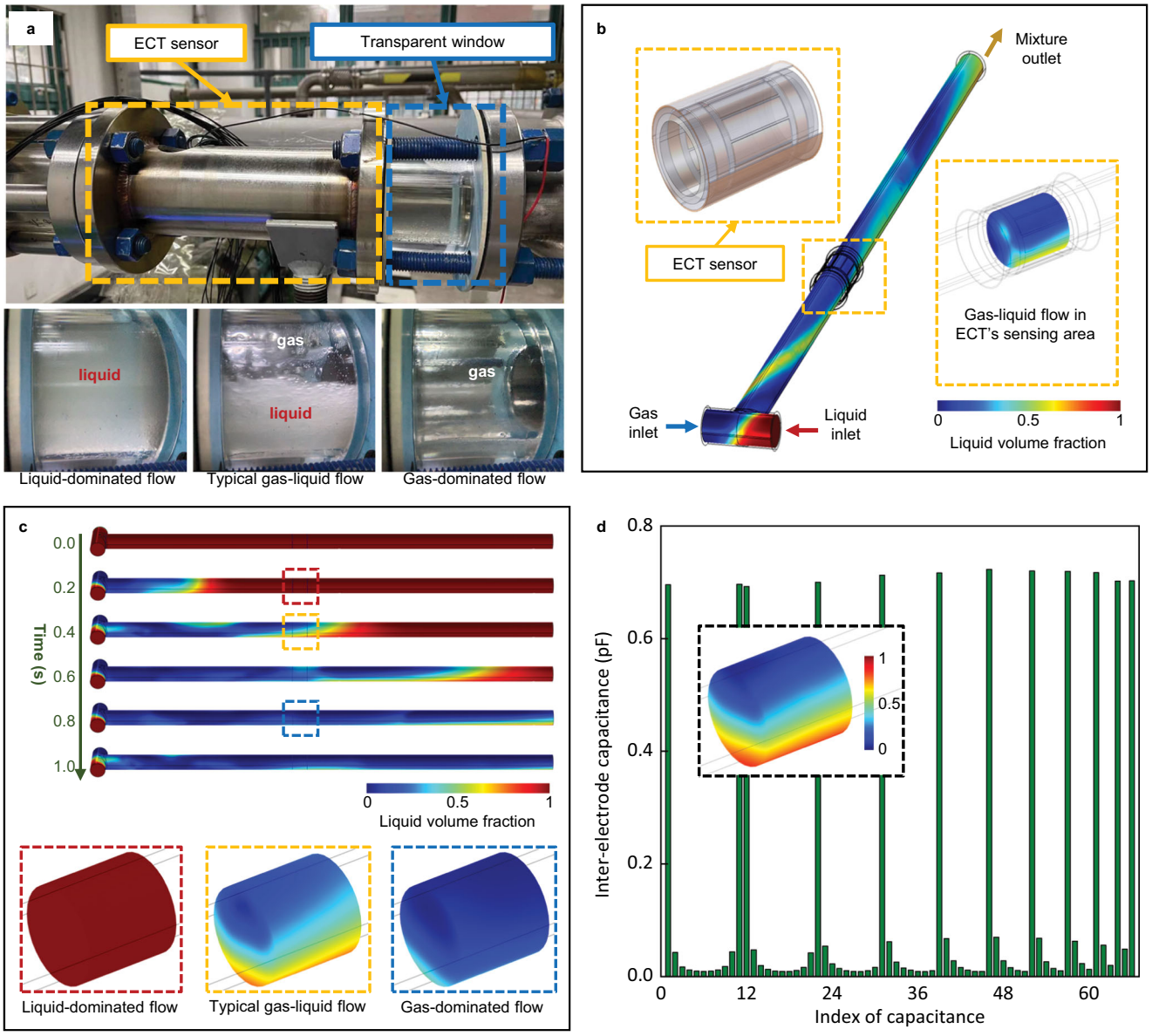

Fig. 2 Three-dimensional coupling simulation of gas-liquid flows. a Physical gas-liquid flows with different volumetric concentrations present in the testing section of the multiphase flow facility. **b** The schematic illustration of the three-dimensional Fluid-Electrostatic field Coupling Model (3D-FECM). Fluid field and electrostatic field are considered to simulate Electrical Capacitance Tomography (ECT) measurements and dynamic gas-liquid flows. **c** Sequential gas-liquid two-phase flows generated by the 3D-FECM. **d** An example of the interelectrode capacitance values obtained by the coupling simulation under a stratified flow.

temporal evolution of the mixture throughout its transient response to varying working conditions.

It is worth pointing out that the ground truth of dynamic multiphase flow profiles in operational flow facilities is in most cases unavailable. As a result, quantitative evaluation of the reconstructed flow images has remained a long-standing yet unsolved challenge. The DT framework presented here addresses this very problem bringing evidence of the capability to visualize and quantify static stratified gas-liquid flows in virtual and physical spaces. We also compare the real-world results with virtual-space results to provide an indicator of the feasibility and performance of the DT framework in the physical world from a quantitative perspective. Figure 5a, b shows the imaging results from the virtual and physical spaces, respectively. We observe that the tomographic images of the virtual static stratified flows and real-world flows are very close to actual distributions. The SSIMs of the images for the virtual static flows are higher than 0.969, and those for the real-world static flows are larger than 0.801, indicating that the DT framework can accurately visualize the gas-liquid flows both in virtual and physical spaces. From the continuous imaging results of gas-liquid flows in the physical facility (see Fig. 5b), we also see that the SSIM result for each working condition is 0.931 ± 0.023, 0.939 ± 0.030, 0.963 ± 0.019, 0.969 ± 0.016 (mean ± standard deviation), respectively. The relative standard uncertainty of the imaging results is better than 3.19%, indicating superior measurement stability and high repeatability of the DT framework.

Discussion

In this study, we introduce the DT concept to multiphase flow imaging systems. We propose a DT framework for ET and demonstrate that it can effectively learn the multiphase flow features in virtual space and provide high resolution and accuracy

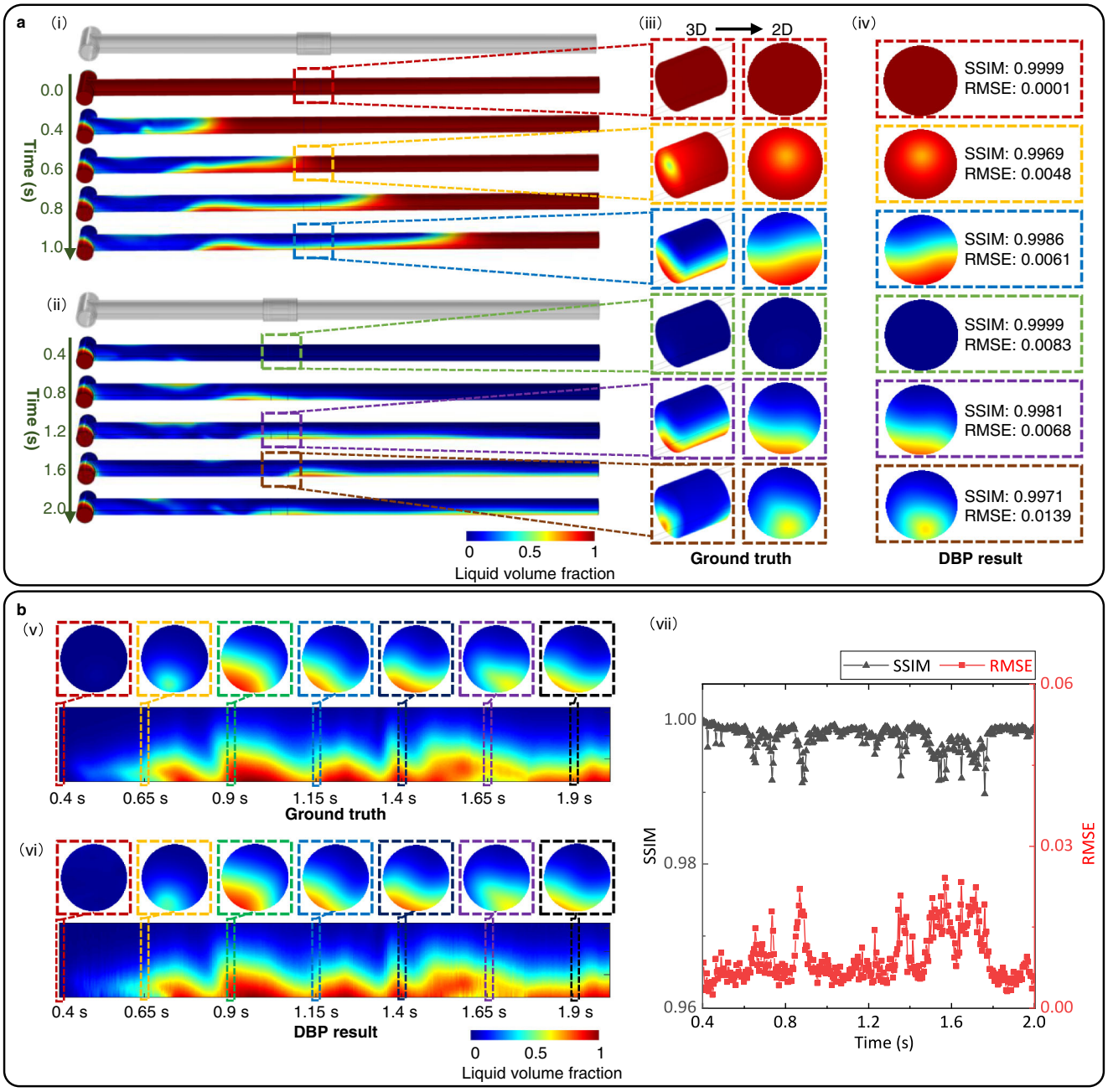

Fig. 3 Quantitative imaging of virtual gas-liquid flows by Deep Back Projection (DBP) with 50 dB Signal-Noise Ratio (SNR). a Two representative sets of sequential gas-liquid flows generated by three-dimensional Fluid-Electrostatic field Coupling Model (3D-FECM) and corresponding image reconstruction results of DBP. For the sequential gas-liquid flows in (i), the pipe is initially filled with liquid. For the sequential gas-liquid flows in (ii), the pipe is initially filled with gas. 3D dynamic liquid phase distributions in the ECT sensing region can be converted to the 2D volume-averaged liquid phase distributions as the ground truth (see (iii)). The cross-section images reconstructed by DBP for the gas-liquid flows in (iii) are presented in (iv). **b** Quantitative imaging of virtual gas-liquid transient flow with high temporal resolution (200 frames per second). (v) The authentic liquid phase distributions for evaluating the performance of image reconstruction. (vi) The images reconstructed by DBP for the gas-liquid flows in (v). The cross-section images in (vi) are a set of representative images selected from the continuous reconstruction results. (vii) The Structural Similarity Index Measure (SSIM) and Root Mean Square Error (RMSE) of the DBP results in (vi).

of multiphase flow imaging in physical space. Despite the superiority of our DT framework, several limitations exist due to current technological bottlenecks and simplistic modeling assumptions.

In virtual space, we leverage 3D-FECM to build the digital representation of the physical multiphase flow imaging system. Coupling the fluid and electrical fields allows simultaneous simulation of dynamic multiphase flows and imaging sensors. However, it is noteworthy that the fundamentals and mathematical treatment of multiphase flow modeling are still the focus of active research[33]. Real-world multiphase flows are among the most complex fluid systems due to the presence of sharp density and velocity gradients across the phases, the strong sensitivity to domain geometrical features and error magnification in the operative conditions. Because of this, achieving a perfect match between the simulation and reality remains an open challenge in

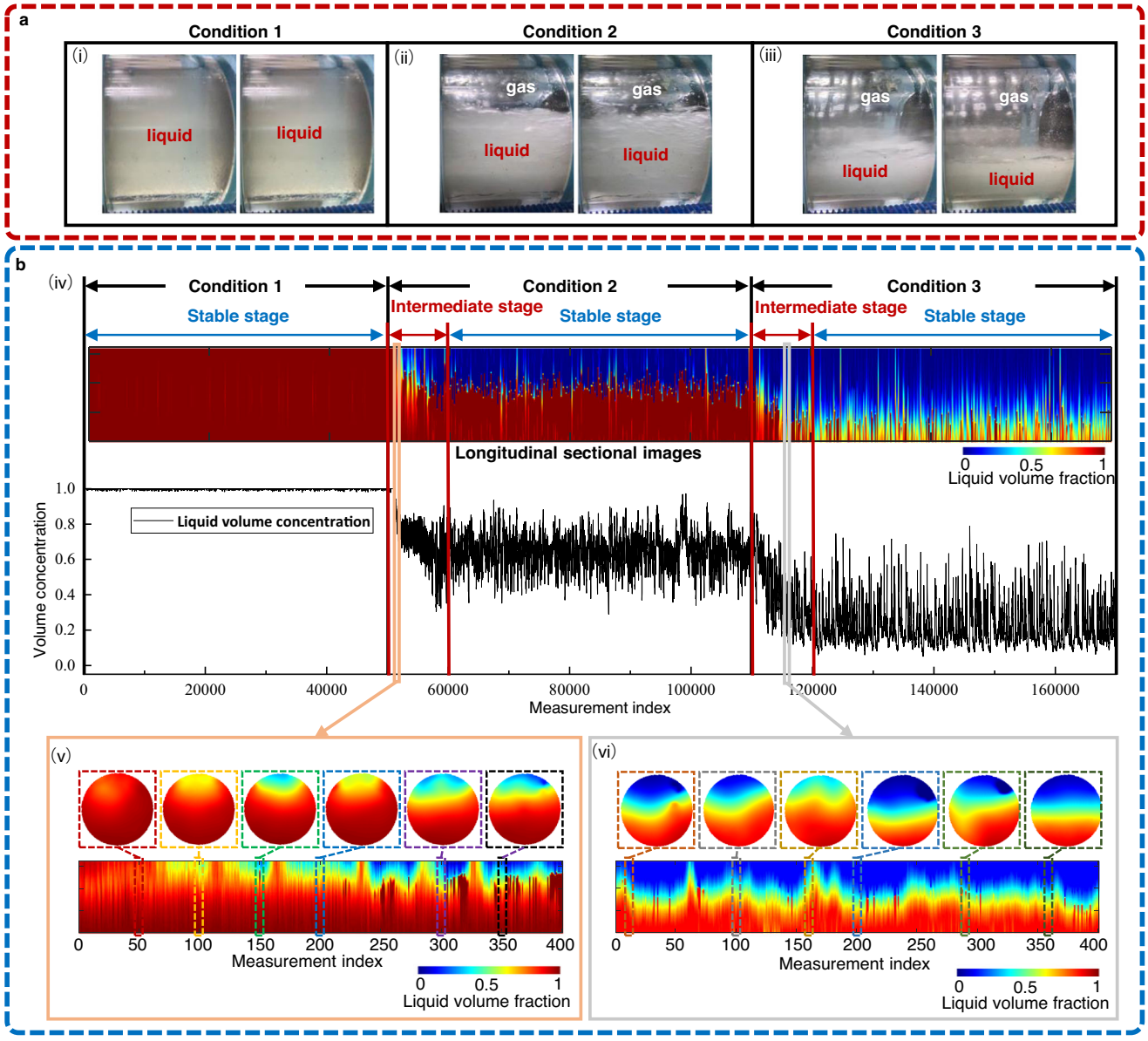

Fig. 4 Tomographic images of gas-liquid flows in the pilot-scale multiphase flow facility under different experimental conditions. In this experiment, three experimental conditions are selected for testing (see Methods for more details). **a** Flow profiles captured by the camera. At the initial stage of the experiment, the pipe is filled with liquid (see (i)). The gas and liquid flow into the testing section with volume flow rates of 20.0 and 5.0 m^3/h, respectively. The gas-liquid two-phase flow with high liquid volumetric concentration is then formed (see (ii)). When the volume flow rate of the gas rises to 100.0 m^3/h and that of the liquid drops to 2.5 m^3/h, the gas-liquid flow with low liquid volumetric concentration is formed (see (iii)). **b** Tomographic images obtained from our Digital Twin (DT) framework. (iv) Tomographic images and liquid volumetric concentration variations of the gas-liquid flows in **a**. Tomographic images in (v) and (vi) show two sets of representative images selected from the time-stacked cross-sectional reconstruction results in (iv).

the multiphase flow modeling community. To mitigate this issue, instead of focusing on the accuracy of the 3D-FECM model to replicate physical multiphase flows, we resort to generating a variety of gas-liquid flows which carry abundant dynamic features that cover a wide range of complex flow conditions in the flow facility. Another limitation of the virtual model is that, although only the testing section is modeled, it still takes extensive time to generate 3D virtual flow and tomographic measurements for each working condition. This is detrimental to the real-time performance of the DT framework. Model optimization to significantly reduce computational cost and leveraging more powerful computing hardware could be a potential solution.

In physical space, we applied our DT framework to visualize dynamic gas-liquid flows in the laboratory-scale multiphase flow facility. However, it was challenging to obtain the ground truth of dynamic gas-liquid flow profiles that could be used for quantitative performance evaluation. Alternatively, we quantitatively evaluated the imaging results of static stratified flows and compared the dynamic imaging results with those captured by high-speed cameras. Static imaging results reveal that the DT framework can visualize real-world gas-liquid flows with high accuracy and excellent repeatability. Future improvements will be to benchmark the experimental performance by incorporating other advanced imaging techniques, e.g., X-ray tomography and MRI, and to compare DT results with these high-precision imaging techniques. Nevertheless, this will involve multi-sensors integration and multi-signal fusion, and the implementation will be complicated and challenging.

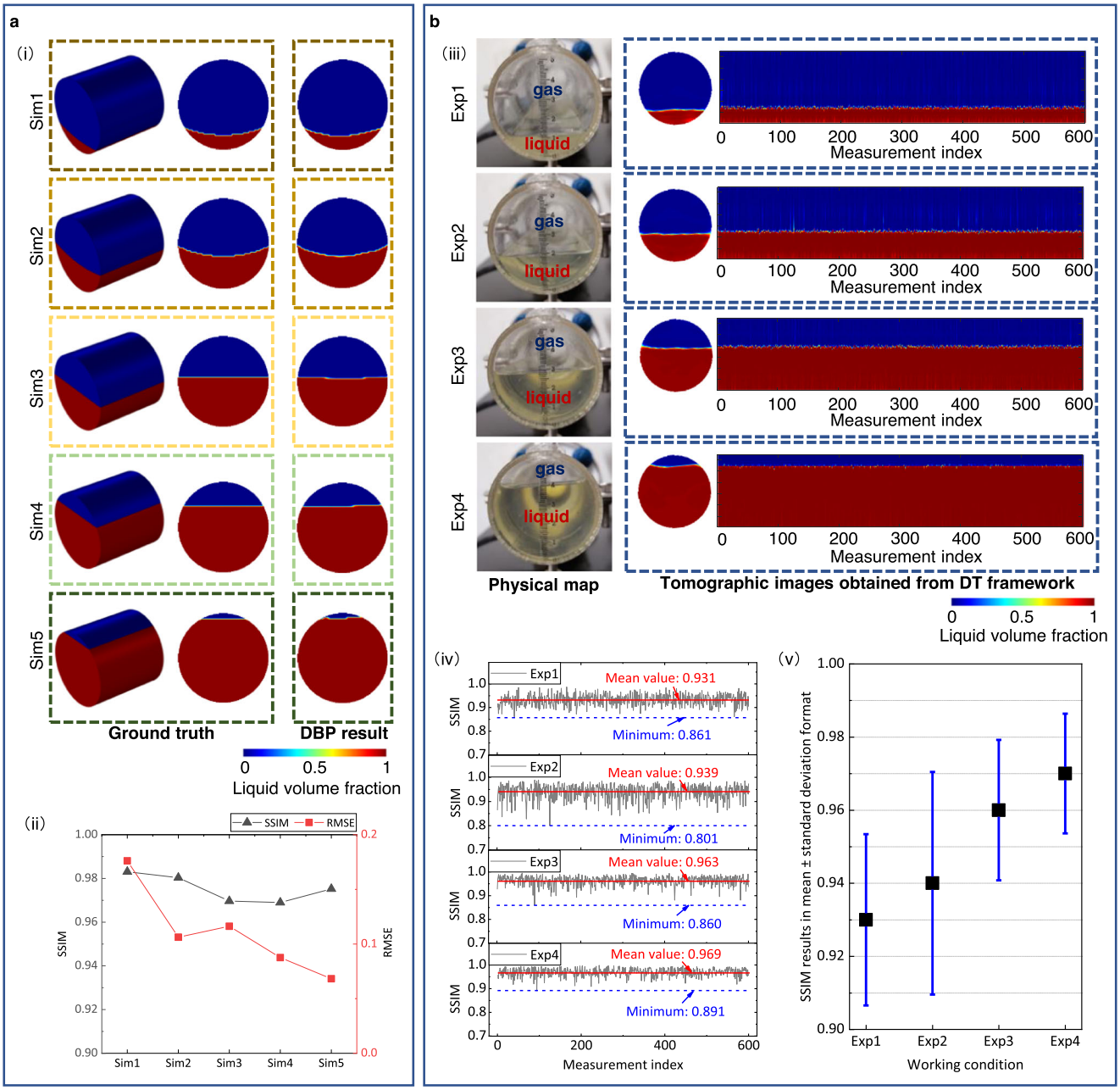

Fig. 5 Evaluation of static stratified gas-liquid flow imaging in virtual and physical spaces. a Imaging static stratified gas-liquid flows in virtual space by Deep Back Projection (DBP) with 50 dB data. (i) Virtual static gas-liquid flows and corresponding image reconstruction results of DBP. (ii) The Structural Similarity Index Measure (SSIM) and Root Mean Square Error (RMSE) of DBP results in (i). **b** Imaging static stratified gas-liquid flows in physical space using DBP. (iii) Real-world static gas-liquid flows and corresponding image reconstruction results of DBP. (iv) The SSIM of the DBP results in (iii). (v) The standard uncertainty of our Digital Twin framework for imaging the real-world static gas-liquid flows in (iii).

It is also noteworthy that the focus of this work is the overall DT framework rather than the learning-based algorithm for ECT image reconstruction. We demonstrate that our DT framework can achieve superior performance even when using simple neural architectures like DBP. We also point out that employing dedicated and more specialized neural architectures can potentially lead to a better performance at the cost of a larger training dataset and a more complex training strategy.

In summary, the proposed DT framework for ET utilizes 3D field-coupling simulation, model-based deep learning, and edge computing to enable precise flow profiles imaging with low-cost, nonradioactive, and noninvasive tomography techniques. We demonstrated substantial improvements of DT-powered ET over conventional ET both virtually and in a pilot-scale multiphase flow facility under various gas-liquid flow conditions. Our DT framework can be trained efficiently and flexibly in the virtual space and be readily implemented in the physical space to provide quantitative and stable imaging of gas-liquid flows, representing a step change compared to the state of the art. The framework is in principle generalizable to various imaging techniques, and emerging real-time simulation/data sketching techniques could realistically propel our DT framework towards widespread multiphase flow imaging applications.

Methods

Multiphase flow facility and experiment design. The testing section of a pilot-scale multiphase flow facility (see Supplementary Fig. S1) at the Multiphase Flow Engineering Laboratory of the Tsinghua International Graduate School is adopted as a case study. The facility consists of a multiphase flow separator, a gas storage tank, gas and liquid single-phase flow sections, the mixing section, and the control system. In this study, the gas-liquid two-phase flow is considered. The working gas and liquid are air (permittivity 1.0, density 1.3 kg m^{-3}) and white oil (permittivity 2.18, density 879 kg m^{-3}), respectively. The oil is separately supplied and pumped into the flow pipe, then blended with the gas in operation. The mixture is transported through the gas-liquid flow testing section and returned to the separator for circulating utilization. A 12-electrode ECT sensor with a transparent window for visual observation is installed in the horizontal mixing section (see Supplementary Fig. S1c). The testing section has an internal diameter of 50 mm, in which gas-liquid two-phase flows with different volumetric concentrations can be formed by manipulating the air and white oil volume flow rates. During the experiment, the working pressure in the testing section is set to 0.6 MPa and the experimental temperature is about 33 °C. The experimental conditions are listed in Supplementary Table S1, where the volume flow rate of white oil varies from 5.0 to 2.5 $m^3 h^{-1}$, and the volume flow rate of air ranges from 20.0 to 100.0 $m^3 h^{-1}$.

3D field-coupling simulation. We created a three-dimensional Fluid-Electrostatic field Coupling Model (3D-FECM) to duplicate the testing section of the flow facility. 3D field-coupling simulation was performed using the commercial software COMSOL Multiphysics and Matlab. The model contains the fluid field interface to generate the gas-liquid flow data and an electrostatic field interface to simulate the 12-electrode ECT sensor. Supplementary Figure S2 shows the flowchart of the 3D field-coupling simulation. We can simultaneously obtain the dynamic permittivity distribution under various flow conditions and corresponding capacitance measurements from the virtual ECT sensor by coupling the fluid field and the electrostatic field.

For the fluid field interface, we employ the laminar two-phase flow, level set method[34] to track the moving interface between the gas and liquid phases. The gas and liquid phases are air and white oil, respectively. We impose the velocity inlet and pressure outlet boundary conditions to avoid convergence difficulties. We select the suppress backflow to prevent fluid from entering the domain through the outlet boundary. The gas-liquid two-phase flow is set as incompressible flow. In line with the experimental setup, the temperature of the simulation environment is set as 33 °C, the dynamic viscosity of the gas and liquid is set as 1.81E-5 and 0.02 Pa.s, respectively, and the density of the gas and liquid is set as 1.3 and 879 kg m^{-3}, respectively.

We apply the Poisson equation[35] to determine the electric potential distribution for the electrostatic field interface. We then use the Wiener Upper Bound formula[36] to evaluate the equivalent permittivity of the gas-liquid mixture. The relative permittivity of the pipe, gas, and liquid is set as 2.6, 1.0, and 2.18, respectively. All the 66 nonredundant interelectrode capacitances are collected for image reconstruction.

Virtual multiphase flow dataset generation. To replicate the real scenarios of the gas-liquid flow testing facility, we initially apply the incompressible Navier-Stokes equations[37] with gravity to simulate gas-liquid two-phase flows in the horizontal section. The dynamic gas and liquid single-phase flows are separately supplied and controlled. Gas-liquid two-phase flow data with different volumetric concentrations are generated by regulating the inlet velocities perpendicular to the entrance surfaces. The inlet liquid velocity varies from 0.071 to 0.708 m s^{-1}, and the inlet gas velocity varies from 0.236 to 2.362 m s^{-1}. To cover a wide range of volumetric concentrations, two initial conditions are set. One is that the pipe is filled with liquid at the initial stage, and the other is that the pipe is filled with gas at the initial stage. We conduct additional virtual dynamic experiments to generate gas-liquid two-phase flows in the microgravity environment to obtain more abundant flow regimes for the machine learning model training. Supplementary Table S2 gives the virtual dynamic experimental matrix. A working condition for the virtual static experiment is also added to generate static stratified gas-liquid flow with the liquid volumetric concentration ranging from 0 to 1. We ran 74 working conditions and collected 12,362 virtual samples containing ECT measurements and phase distributions.

DBP for quantitative flow imaging. We found that the conventional Linear Back Projection (LBP) algorithm[29] is the most effective in reconstructing dynamic flow profiles than iterative algorithms. We therefore further refine the LBP results with machine learning. DBP is a model-based deep learning algorithm designed to quantitatively image the flow profiles (see Supplementary Fig. S5 for the network structure). Here, we consider the commonly used ECT model[29], i.e.,

$$\lambda = Sg \tag{1}$$

where λ denotes the normalized capacitance measurement vector; S is the Jacobian matrix; and g represents the normalized permittivity distribution within the Region of Interest (ROI).

Reconstruction of the flow distribution with DBP involves two steps. First, the normalized measurement vector λ is mapped into a coarse flow distribution g_{LBP} based on the LBP algorithm[29]. Then, a modified UNet[38] is applied to refine the LBP result and produce a more accurate image g_U.

DBP is implemented in Pytorch. The Adam optimizer[39] is used to update network parameters. The hyperparameters of Adam are set as: $\beta_1 = 0.9$, $\beta_2 = 0.999$, $\epsilon = 10^{-9}$, weight decay = 0. The initial learning rate is 0.001, which decays every 2 epochs with a factor of 1.111. The simulation data is divided into three groups, i.e., the training, validation, and testing sets. The training set includes 10,505 samples (62 different flow conditions at normal time resolution in the dynamic simulation and 89 different flow conditions in the static simulation). The validation set includes 1680 samples (10 different flow conditions at normal time resolution in the dynamic simulation). The testing set includes 1380 samples (one flow condition at normal time resolution, three flow conditions at high time resolution in the dynamic simulation, and nine different flow conditions in the static simulation). All data are augmented by 3 noise levels (i.e., 40, 50, and 60 dB). We select mean square error as the loss function. The batch size and the number of epochs are set to 25 and 80, respectively. The whole training takes about 3 h on three Nvidia Quadro P5000 GPUs. The network with the least validation loss is selected as our final model, which can achieve 0.996 ± 0.012 (mean ± standard deviation) for SSIM, 0.005 ± 0.008 (mean ± standard deviation) for RMSE, and 40.218 ± 1.701 (mean ± standard deviation) for Peak Signal to Noise Ratio (PSNR) on the whole testing set.

AI-powered tomography system. The trained DBP is implemented in the AI-powered electrical tomography system in the physical space. We use ECT to demonstrate the construction of the AI-power tomography system. However, the architecture could be easily extended to other electrical tomography modalities. The AI-powered ECT system is composed of a 32-channel ECT hardware[30,40], an edge AI computer (NVIDIA Jetson Nano), and a Visual Tomography (VT) software integrating the trained DBP model for real-time quantitative flow profile reconstruction and key parameter prediction (see Supplementary Fig. S10 for the system architecture). The ECT hardware is interfaced with the Jetson Nano through a USB2.0 port. The VT software developed via Python is implemented on Jetson Nano for ECT measurement control, data collection, image reconstruction, and visualization. It also provides an interface to update the trained DBP model dynamically and remotely.

Data availability

We have uploaded the virtual multiphase flow dataset to the Edinburgh DataShare, accessible at: https://doi.org/10.7488/ds/3501. The data that support the findings of this study are available from the corresponding author upon reasonable request.

Code availability

Code to replicate this research can be available from the corresponding author upon reasonable request.

Received: 13 June 2022; Accepted: 24 November 2022;
Published online: 02 December 2022

References

1. Sheng, Z. Z. et al. Liquid gating elastomeric porous system with dynamically controllable gas/liquid transport. *Sci. Adv.* https://doi.org/10.1126/sciadv.aao6724 (2018).
2. Hou, X., Hu, Y. H., Grinthal, A., Khan, M. & Aizenberg, J. Liquid-based gating mechanism with tunable multiphase selectivity and antifouling behaviour. *Nature* **519**, 70–73 (2015).
3. Balachandar, S. & Eaton, J. K. Turbulent dispersed multiphase flow. *Ann. Rev. Fluid Mech.* **42**, 111–133 (2010).
4. Wang, Q. Q. et al. Ultrasound Doppler-guided real-time navigation of a magnetic microswarm for active endovascular delivery. *Sci. Adv.* https://doi.org/10.1126/sciadv.abe5914 (2021).
5. Li, Z. G. et al. Flow regime transition in countercurrent packed column monitored by ECT. *Chem. Eng. J.* https://doi.org/10.1016/j.cej.2021.129841 (2021).
6. Sloan, E. D. Fundamental principles and applications of natural gas hydrates. *Nature* **426**, 353–359 (2003).
7. Thampi, S. P., Doostmohammadi, A., Shendruk, T. N., Golestanian, R. & Yeomans, J. M. Active micromachines: microfluidics powered by mesoscale turbulence. *Sci. Adv.* https://doi.org/10.1126/sciadv.1501854 (2016).
8. Shaw, R. A. Particle-turbulence interactions in atmospheric clouds. *Ann. Rev. Fluid Mech.* **35**, 183–227 (2003).

9. Shi, X. W., Tan, C., Dong, F., dos Santos, E. N. & da Silva, M. J. Conductance sensors for multiphase flow measurement: a review. *IEEE Sens. J.* **21**, 12913–12925 (2021).
10. Aliseda, A. & Heindel, T. J. X-ray flow visualization in multiphase flows. *Annual Review of Fluid Mechanics* **53**, 543–567 (2021).
11. Heindel, T. J. A review of X-ray flow visualization with applications to multiphase flows. *J. Fluids Eng. Transac. Asme* https://doi.org/10.1115/1.4004367 (2011).
12. Hu, B., Langsholt, M., Liu, L., Andersson, P. & Lawrence, C. Flow structure and phase distribution in stratified and slug flows measured by X-ray tomography. *Int. J. Multiphase Flow* **67**, 162–179 (2014).
13. Lakshmanan, S., Maru, W. A., Holland, D. J., Mantle, M. D. & Sederman, A. J. Measurement of an oil-water flow using magnetic resonance imaging. *Flow Measure. Instrum.* **53**, 161–171 (2017).
14. Yao, J. F. & Takei, M. Application of process tomography to multiphase flow measurement in industrial and biomedical fields: a review. *IEEE Sens. J.* **17**, 8196–8205 (2017).
15. York, T., McCann, H. & Ozanyan, K. B. Agile sensing systems for tomography. *IEEE Sens. J.* **11**, 3086–3105 (2011).
16. Huang, Y. H. et al. Noninvasive visualization of electrical conductivity in tissues at the micrometer scale. *Sci. Adv.* https://doi.org/10.1126/sciadv.abd1505 (2021).
17. Dyakowski, T., Jeanmeure, L. F. C. & Jaworski, A. J. Applications of electrical tomography for gas-solids and liquid-solids flows—a review. *Powder Technol.* **112**, 174–192 (2000).
18. Warsito, W. & Fan, L. S. Neural network based multi-criterion optimization image reconstruction technique for imaging two- and three-phase flow systems using electrical capacitance tomography. *Measure. Sci. Technol.* **12**, 2198–2210 (2001).
19. Ravagli, E. et al. Imaging fascicular organization of rat sciatic nerves with fast neural electrical impedance tomography. *Nat. Commun.* https://doi.org/10.1038/s41467-020-20127-x (2020).
20. Aidun, C. K. & Clausen, J. R. Lattice-Boltzmann method for complex flows. *Annu. Rev. Fluid Mech.* **42**, 439–472 (2010).
21. Jordan, M. I. & Mitchell, T. M. Machine learning: trends, perspectives, and prospects. *Science* **349**, 255–260 (2015).
22. Corbetta, A., Menkovski, V., Benzi, R. & Toschi, F. Deep learning velocity signals allow quantifying turbulence intensity. *Sci. Adv.* https://doi.org/10.1126/sciadv.aba7281 (2021).
23. Wei, Z. & Chen, X. D. Induced-current learning method for nonlinear reconstructions in electrical impedance tomography. *IEEE Transac. Med. Imaging* **39**, 1326–1334 (2020).
24. Li, F., Tan, C. & Dong, F. Electrical resistance tomography image reconstruction with densely connected convolutional neural network. *IEEE Transac. Instrum. Measure.* https://doi.org/10.1109/tim.2020.3013056 (2021).
25. Xiang, J. X., Dong, Y. G. & Yang, Y. J. FISTA-Net: learning a fast iterative shrinkage thresholding network for inverse problems in imaging. *IEEE Transac. Med. Imaging* **40**, 1329–1339 (2021).
26. Li, F., Tan, C., Dong, F. & Jia, J. B. V-Net deep imaging method for electrical resistance tomography. *IEEE Sens. J.* **20**, 6460–6469 (2020).
27. Liu, S. H., Huang, Y. M., Wu, H. C., Tan, C. & Jia, J. B. Efficient multitask structure-aware sparse bayesian learning for frequency-difference electrical impedance tomography. *IEEE Transac. Industrial Inf.* **17**, 463–472 (2021).
28. Xiang, J. X., Dong, Y. G. & Yang, Y. J. Multi-frequency electromagnetic tomography for acute stroke detection using frequency-constrained sparse bayesian learning. *IEEE Transac. Med. Imaging* **39**, 4102–4112 (2020).
29. Yang, W. Q. & Peng, L. H. Image reconstruction algorithms for electrical capacitance tomography. *Measure. Sci. Technol.* **14**, R1–R13 (2003).
30. Yang, Y. J., Peng, L. H. & Jia, J. B. A novel multi-electrode sensing strategy for electrical capacitance tomography with ultra-low dynamic range. *Flow Measure. Instrum.* **53**, 67–79 (2017).
31. Wang, Z., Bovik, A. C., Sheikh, H. R. & Simoncelli, E. P. Image quality assessment: from error visibility to structural similarity. *IEEE Transac. Image Process.* **13**, 600–612 (2004).
32. Shi, X. W., Tan, C., Wu, H. & Dong, F. An electrical and ultrasonic doppler system for industrial multiphase flow measurement. *IEEE Transac. Instrum. Measure.* https://doi.org/10.1109/tim.2020.3013080 (2021).
33. Subramaniam, S. Multiphase flows: rich physics, challenging theory, and big simulations. *Phys. Rev. Fluids* https://doi.org/10.1103/PhysRevFluids.5.110520 (2020).
34. Olsson, E. & Kreiss, G. A conservative level set method for two phase flow. *J. Comput. Phys.* **210**, 225–246 (2005).
35. Grochowski, P. & Trylska, J. Review: Continuum molecular electrostatics, salt effects, and counterion binding-a review of the Poisson-Boltzmann theory and its modifications. *Biopolymers* **89**, 93–113 (2008).
36. Liu, N. T. & Jin, Y. Q. A discussion on the effective permittivity of multi-component medium derived by Maxwell-Garnett, strong fluctuation and quasicrystalline-CP modeling. *Waves Random Complex Media* **31**, 1921–1930 (2021).
37. Brown, D. L., Cortez, R. & Minion, M. L. Accurate projection methods for the incompressible Navier-Stokes equations. *J. Comput. Phys.* **168**, 464–499 (2001).
38. Guan, S., Khan, A. A., Sikdar, S. & Chitnis, P. V. Fully dense UNet for 2-D sparse photoacoustic tomography artifact removal. *IEEE J. Biomed. Health Inform.* **24**, 568–576 (2020).
39. Gopalakrishnan, K., Khaitan, S. K., Choudhary, A. & Agrawal, A. Deep Convolutional Neural Networks with transfer learning for computer vision-based data-driven pavement distress detection. *Construct. Build. Mater.* **157**, 322–330 (2017).
40. Yang, Y. J. & Peng, L. H. A configurable electrical capacitance tomography system using a combining electrode strategy. *Measurem. Sci. Technol.* https://doi.org/10.1088/0957-0233/24/7/074005 (2013).

Acknowledgements

This work is financially supported by European Union's Horizon 2020 Research and Innovation Programme under the Marie Sklodowska-Curie actions COFUND Trans-national Research and Innovation Network at Edinburgh Grant 801215, Research Institute of Tsinghua, Pearl River Delta, LeEngStar Technology Co., Ltd, Data Driven Innovation Chancellor's Fellowship, and National Natural Science Foundation of China Grant 51906209.

Author contributions

Y.Y. conceived the idea and supervised the entire project. S.W. developed the 3D field-coupling simulation framework, generated the virtual sensing data, carried out data analysis, and led the the writing of the manuscript. D.H. and J.Q. developed the DBP network and conducted data analysis. M.Z. and Y.L. managed experiments and data collection. W.C. conducted static experiments. F.G.S. supervised the fluid simulation. L.P. supervised the electrical tomography parts and measurement system design. All the authors participated in discussions of the results and contributed to the writing of the manuscript.

Competing interests

The authors declare no competing interests.

Additional information

Supplementary information The online version contains supplementary material available at https://doi.org/10.1038/s44172-022-00042-3.

Correspondence and requests for materials should be addressed to Yunjie Yang.

Reprints and permission information is available at http://www.nature.com/reprints

Publisher's note Springer Nature remains neutral with regard to jurisdictional claims in published maps and institutional affiliations.